Available online at www.sciencedirect.com
SCIENCE DIRECT®
Journal of Electron Spectroscopy and Related Phenomena 148 (2005) 151–157
JOURNAL OF ELECTRON SPECTROSCOPY and Related Phenomena
www.elsevier.com/locate/elspec

Near edge X-ray absorption fine structure (NEXAFS) of model compounds for the humic acid/actinide ion interaction

Markus Plaschke *, Jörg Rothe, Marcus Altmaier, Melissa A. Denecke, Thomas Fanghänel

Forschungszentrum Karlsruhe GmbH, Institut für Nukleare Entsorgung, Postfach 3640, D-76021 Karlsruhe, Germany

Received 22 December 2004; received in revised form 3 May 2005; accepted 9 May 2005
Available online 24 June 2005

Abstract

To understand spectral features of humic acid (HA) C 1s-near edge X-ray absorption fine structure (NEXAFS) with and without metal ion complexation, a set of model compounds is investigated. Halogenated benzoic acids and anthranilic acid are examined to demonstrate the effect of electron withdrawing groups on the C 1s-NEXAFS spectra of complex organic acids, including HA. The peak positions for aromatic and carboxylic groups in these spectra are in agreement with common assignments. The spectral position of the peak for substituted aromatic carbon shifts with increasing electronegativity of the substituent to higher photon energies. Polyacrylic acid (PAA) and different PAA metal ion complexes are investigated as model substances for metal cation complexation by HA. Tb(III)-, Zr(IV)- and U(VI)–PAA exhibit general spectral signatures previously observed for the PAA/Eu(III)–PAA system. For these different metal cations, similar spectral changes and distinct variations in peak intensities are observed going from the uncomplexed to the metal-loaded macromolecules. These spectral changes are comparable to those for U(VI)- and Th(IV)–HA systems.

Keywords: Humic acid; Polyacrylic acid (PAA); Scanning transmission X-ray microscopy (STXM); C 1s-NEXAFS; Substituted benzoic acid

1. Introduction

Humic acids (HA) comprise a class of natural organic matter especially stable against bio- and geochemical alteration. HA are water-soluble biopolymers with dimensions in the nanometer range and an inherent chemical poly-functionality [1]. These chemical and size properties are responsible for HA ability to bind and transport trace metal ions in natural aquifers. Therefore, HA may play a significant role in the far-field transport of radionuclides, i.e. actinide ions potentially released from a nuclear waste repository [2]. Depending on the geochemical milieu, actinides may as well form oxo/hydroxide colloids (generated by hydrolysis and subsequent poly-nucleation) [3] or adsorb on inorganic aquatic colloids, e.g. clays [4]. The chemical properties and colloidal stability of these inorganic particles may be altered by surface reactions with HA. As part of the overall assessment of the impact of HA on actinide transport phenomena, it is mandatory to characterize both the nature of HA/actinide ion complexes and HA hetero-aggregates with actinide oxo/hydroxide colloids.

Soft X-ray spectroscopy and spectromicroscopy studies have great potential to provide insight into HA interactions with trace metal ions (Me^{n+}) and inorganic colloids [5–8]. The present paper is a continuation of a previous study employing scanning transmission X-ray microscopy (STXM) to study Me^{n+}–HA complexation by comparison to model systems [9]. This approach aims at interpreting C 1s-near edge X-ray absorption fine structure (NEXAFS) of Me^{n+}-reacted HA by comparison to spectral signatures of structurally well-defined organic model substances. The selected model compounds comprise simple organic acids representing possible HA building blocks and water-soluble polymers acting as model systems for metal ion complexation. Substituted benzoic acids are appropriate model

* Corresponding author. Tel.: +49 7247 82 4747; fax: +49 7247 82 3927.
E-mail address: plaschke@ine.fzk.de (M. Plaschke).

0368-2048/$ – see front matter © 2005 Elsevier B.V. All rights reserved.
doi:10.1016/j.elspec.2005.05.001

compounds to test the validity of the 'functional group fingerprinting' approach commonly used to interpret spectra of complex natural biopolymers [9]. Their C 1s-NEXAFS exhibits strong π^* transitions assigned as aromatic, substituted aromatic and carboxylic carbon functionalities, resembling those of HA. It is known from previous extended X-ray absorption fine structure (EXAFS) studies that the carboxyl functions act as primary metal ion complexing sites in HA [10,11]. Therefore, polyacrylic acid (PAA) is chosen as a simple but appropriate model compound. PAA is water-soluble, has a high content of carboxyl functional groups and a simple chemical structure with variable chain length. In our previous study, striking similarities are found in spectral trends of the C 1s-NEXAFS signatures before and following complexation with Eu(III) for the PAA/Eu(III)–PAA and HA/Eu(III)–HA systems [9]. If the strong spectral changes observed to be associated with metal ion complexation are unambiguously established for different model systems, it may be possible to identify the specific electronic environment of carbon in the functional groups responsible for Me^{n+} complexation in HA.

We are presently establishing an experimental data base of model compounds. The compounds in this study represent an addition to this data base. Selection of substituted benzoic acids emphasizes the variation of structural subunits inducing C 1s-NEXAFS spectral resonances at energies intermediate between the aromatic and the carboxylic transition. Changes in NEXAFS spectra for PAA and HA following Me^{n+} complexation are observed in this energy range. Halogen substituted benzoic acids are investigated to study the effect of electron withdrawing groups with different electronegativities on the C 1s-NEXAFS. In addition, the complexation effect previously observed in the NEXAFS of Eu(III)–PAA is investigated for other metal cations, including—for the first time—actinide cations.

2. Experimental

2.1. Sample preparation

All chemicals are of analytical grade (purchased from Sigma–Aldrich, Deisenhofen, Germany) unless specified otherwise. A droplet of 1 μL aqueous sample solution of 2-, 3- and 4-substituted fluoro-, chloro-, bromo- and iodobenzoic and anthranilic acid (all concentrations around 2 g/L) is pipetted onto a silicon nitride window and air-dried. A similar sample preparation is used for polyacrylic acid (PAA, Na-form, calibration standard, molecular weight M_W ~83,400; 1 g/L). For the investigation of Me^{n+}–PAA, complexation acidic solutions (pH ~2) of nitrate salts of Eu(III), Tb(III) and Zr(IV) (diluted ICP-MS standards) are added to acidic PAA solutions (in 0.1 M NaCl, Merck Suprapur, Darmstadt, Germany) and the pH is carefully adjusted by addition of small portions of 0.1 M NaOH to the values given in Table 1. The U(VI)–PAA sample is prepared similarly using a 1E−3 M stock solution of uranyl nitrate hexahydrate (Merck, Darmstadt, Germany) in 0.1 M NaCl (pH 4). The final total Me^{n+} concentrations (c Me^{n+}) and pH values of the Me^{n+}–PAA sample solutions are given in Table 1. Note that for U(VI)- and Zr(IV) solutions, a considerable amount of Me^{n+} may be present as hydrolyzed or polynuclear species. In all Me^{n+}–PAA solutions, a white precipitate is formed.

Table 1
Compositions of the Me^{n+}–PAA/HA sample solutions (in 0.1 M NaCl)

Sample	c PAA/HA (g/L)	c Me^{n+} (mol/L)	pH
Eu(III)–PAA	1.9	3.1E−2	4.9
Tb(III)–PAA	0.2	5.0E−3	5.1
U(VI)–PAA	0.03	6.0E−4	4.6
Zr(IV)–PAA	0.08	8.4E−4	4.0
U(VI)–HA	0.18	1.0E−4	4.3
Th(IV)–HA	0.2	1.0E−4	5.3

Commercial Aldrich HA (Deisenhofen, Germany) is purified according to a procedure described by Kim et al. [12]. A stock solution of 400 mg/L HA, with an electrolyte content of 0.1 M NaCl, is prepared, adjusted to pH 6.0 and stored at 5 °C. The aforementioned U(VI) solution is also used for preparation of U(VI)–HA. A 4E−3 M Th-nitrate solution (Merck, Darmstadt) in 0.1 M NaCl (pH 5.5) is used for preparing the Th(IV)–HA sample. Under these conditions, a voluminous precipitate of Th(IV)-hydroxide is formed. The supernatant is dominated by Th(IV)-oxo/hydroxide colloids [3]. The actinide containing solutions are added to the HA solutions and adjusted to the final concentrations and pH in Table 1. After addition of actinide solutions to the HA stock solution, rapid flocculation is observed.

Me^{n+}–PAA and Me^{n+}–HA aqueous suspensions are investigated as thin films using silicon nitride wet cells. This sample preparation technique for STXM measurements using wet cells has been described elsewhere [13].

2.2. Scanning transmission X-ray microscopy

Soft X-ray spectromicroscopy investigations are performed at the STXM endstation (X-1A Outboard-STXM) at the National Synchrotron Light Source, Brookhaven, NY [14]. At the X-1A Outboard-STXM, a Fresnel zone plate is used to focus the undulator beam into a spot of soft X-rays. The zone plate has a diameter of 160 μm and a width of 45 nm of the outer most ring segment, giving a resolution (Rayleigh criterion) of 55 nm [15]. The STXM endstation provides a flux of about 10^7 photons/s, with an energy bandwidth of about 0.1 eV at the C 1s-energy (see, e.g. [13] and references therein). The spherical grating monochromator (SGM) is calibrated against the C 1s-absorption threshold resonance of carbon dioxide at 292.76 eV. Pseudo-Voigt profile curve-fitting of this transition peak indicates that spectral line widths down to 0.5–0.6 eV FWHM (including contributions from natural line width and instrumental broadening) can be resolved with the experimental setup.

Stacks of images from selected sample regions are recorded as a function of incident photon energy E. For a

review of the procedure for image stack data analysis, see Ref. [16]. In this study, stacks of 115 images are recorded at E ranging between ~280 and 305 eV. E is varied for recording images in 1 eV steps in the range 280–283 eV, in 0.1 eV steps for 283–292 eV, in 0.5 eV steps at energies 292–300 eV and in 1 eV steps at energies 300–305 eV. C 1s-NEXAFS spectra are extracted through the analysis of the absorption signal, $\mu(E) \times d = \ln(I_0(E)/I(E))$, of vertical projections onto aligned image stacks. Image regions free of particles supply information on the I_0 signal. The transmitted intensity (I) is derived from image regions containing carbonaceous structures. Details of an X-ray absorption spectrum such as sharp features in the C 1s-NEXAFS are dependent upon the thickness of the absorbing layer [17]. Hence, sample zones with 40–70% transmission were selected for extraction of the spectra, minimizing possible thickness effects [18]. A linear pre-edge background (280–283 eV) is subtracted from the extracted spectra, followed by normalization ($\mu \times d = 1$) at 300 eV. Normalization artifacts in the spectral region of about 282–286 eV, due to a strong dip in the I_0 signal (caused by carbon deposits on mirrors and the SGM), cannot be entirely ruled out. To estimate a potential influence of sample damage by the soft X-rays during image acquisition, a 'coarse' spectrum with low energy resolution (from 10 images at 10 selected energy positions) is recorded before and after each spectral image stack. Any changes observed in optical density would be an indication of radiation damage.

Table 2
Peak assignments and energy positions (in eV) for C 1s → π* transitions of the substituted benzoic acids

Peak assignment (energy ranges in Fig. 1)	C═C (*A*)	C─X (*B*)	C═O (*C*)
Benzoic acid[a]	284.9	–	288.2
4-Hydroxobenzoic acid[a]	285.0	286.8	288.3
4-Aminobenzoic acid[b]	285.0	286.5	288.4
4-Fluorobenzoic acid	285.1	287.1	288.4
2-Fluorobenzoic acid	285.0	287.2	288.2
4-Chlorobenzoic acid	285.1	286.1	288.3
2-Chlorobenzoic acid	284.9	286.2	288.2
4-Bromobenzoic acid	285.1	285.9	288.3
2-Bromobenzoic acid	284.9	286.0	288.3
4-Iodobenzoic acid	285.0	285.6	288.4
3-Iodobenzoic acid	285.0	285.7	288.4
2-Iodobenzoic acid	284.8	285.6	288.3

[a] From Ref. [9].
[b] Anthranilic acid.

3. Results and discussion

3.1. NEXAFS spectra of substituted benzoic acids

The C 1s-NEXAFS spectra of 4-substituted benzoic acids (4-hydroxy-, 4-amino-, 4-fluoro-, 4-chloro-, 4-bromo- and 4-iodobenzoic acid) are displayed in Fig. 1 and their peak positions are summarized in Table 2 (including values for the 2- and 3-substituted benzoic acids investigated, spectra not shown). The spectra exhibit sharp peaks due to local-

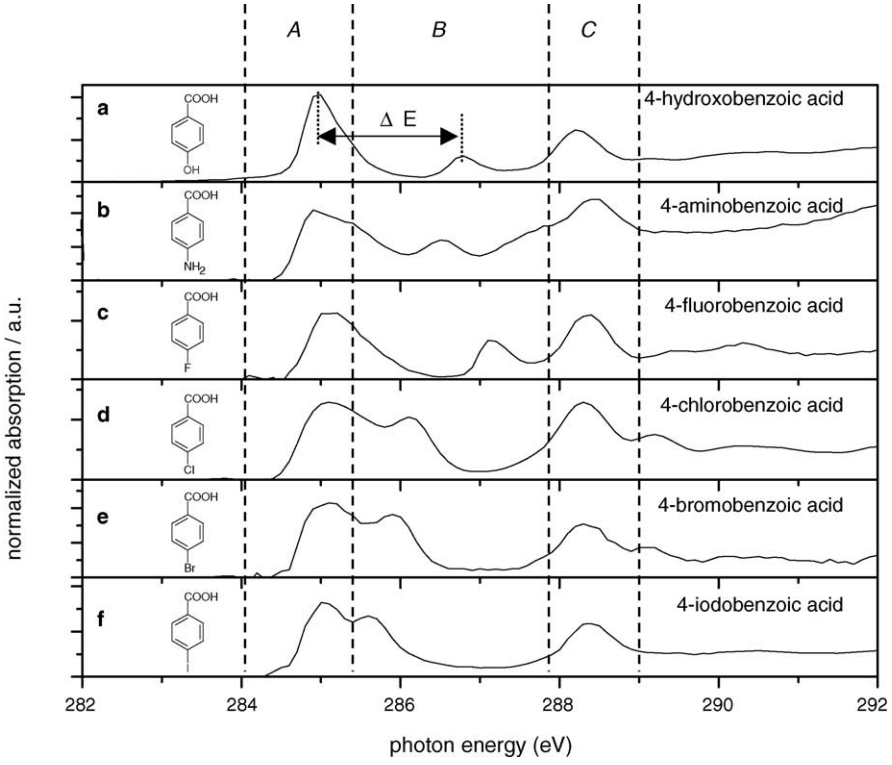

Fig. 1. Normalized C 1s-NEXAFS spectra of 4-halogen-, hydroxyl- and amino-substituted benzoic acids (see Table 2 for assignments, ΔE is difference between the NEXAFS peak positions of the aromatic (C─H) and substituted aromatic carbon (C─X) transition, see Fig. 2).

ized 1s → π* transitions between about 284 and 289 eV (i.e. below the C 1s ionization potential) followed by broad features representing multi-electron excitations, as well as 'shape resonances' (1s → σ* transitions), leading to the continuum part beyond 290 eV. The following discussion will be restricted to the most prominent 1s → π* transitions in the discrete part of the spectra. In agreement with the literature, the transitions in energy ranges *A*, *B* and *C* in Table 2 and Fig. 1 are assigned to aromatic, substituted aromatic and carboxylic carbon, respectively [19].

Each compound in Fig. 1 consists of an aromatic ring with a single carboxyl group and a substituted aromatic carbon in the para ring position to the carboxyl group. The C=O double bond in these molecules is visible as the C 1s (COOH) → $\pi^*_{C=O}$ transition at ∼288.3 eV (carboxyl peak, energy position *C*). Peak location, intensity and width are nearly identical for all six spectra (Fig. 1). For the 12 compounds summarized in Table 2, a mean value of the carboxyl peak of 288.3 ± 0.1 eV is found; the transition energy is constant within the spectrometer resolution. The carbon atoms at the unsubstituted benzene ring sites (ring positions 2, 3, 5 and 6) are reflected by their C 1s (C–H) → $\pi^*_{C=C}$ transitions at ∼285.0 eV (aromatic peak, energy position *A*). As for hydroxyl substituted benzoic acids [9], a significant broadening of this peak (line width >1 eV) compared to the CO_2 π* transition is observed (cf. Section 2). This reflects that the varying site symmetries of benzene ring carbon atoms possess site specific C 1s → π* transitions. For the compounds in Fig. 1, the transitions of the unsubstituted ring carbons (C–H) are grouped in an experimentally unresolved energy range, leading to the broad 'aromatic' peak. It is assumed that the C 1s (C–COOH) → $\pi^*_{C=C}$ transition is located at the high energy tailing edge of the aromatic peak [9]. A high energy tailing of the aromatic peak is observed for all these substituted benzoic acids, provided the aromatic peak is separated from transitions of substituted aromatic carbon. The aromatic peak maximum of the 12 compounds in Table 2 is at 285.0 ± 0.1 eV, which is again constant within the spectrometer resolution.

The peak associated with the substituted aromatic carbon (C 1s (C–X) → $\pi^*_{C=C}$ transition, energy range *B*) is observed to vary with the substituent (X = OH, NH_2, F, Cl, Br and I). The position of this peak correlates with the electronegativity of the substituent atom: F (287.1 eV) > O (286.8 eV) > N (286.5 eV) > Cl (286.1 eV) > Br (285.9 eV) > I (285.6 eV). In Fig. 2, the electronegativity of the substituent atoms X (after Allred and Rochow, e.g. [20]) is plotted as a function of the relative NEXAFS peak position (defined as the energy shift, Δ*E*, between the peak position of the substituted aromatic carbon C–X and the aromatic carbon C–H). A linear correlation (*R* = 0.95) between the electronegativity and Δ*E* is evident (filled circles and line in Fig. 2). A similar electron withdrawing effect is reported for ^{13}C NMR spectra of halogen substituted benzoic acids. The correlation between Δ*E* (NEXAFS) and Δ ppm (^{13}C NMR) is shown in Fig. 2 (symbolized by open triangles). Δ ppm is defined as

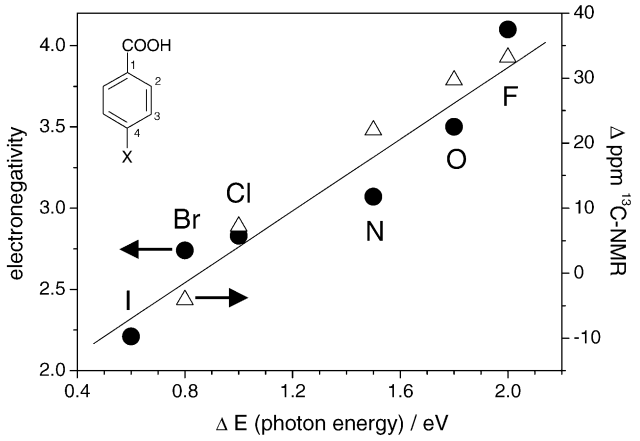

Fig. 2. Correlation between Δ*E* of 4-substituted benzoic acids (see Fig. 1) and the elemental electronegativity of the substituent atom X = F, O, N, Cl, Br and I (left *y*-axis, symbol (●), linear correlation shown) and between Δ*E* and the difference chemical shift Δ ppm in ^{13}C NMR (right *y*-axis, symbol Δ); Δ ppm is the difference between the ^{13}C NMR chemical shifts of C–H and C–X (^{13}C NMR data are taken from Ref. [21]; see text).

the difference between the chemical shift of the C–H and the C–X group at ring positions 2 and 4, respectively (^{13}C NMR chemical shifts are taken from [21]). In both methods, the chemical shift is primarily related to the electronegativity of the substituent atom. Similar correlations have been reported for C 1s-electron energy loss spectroscopy (EELS) spectra of mono-halogenated benzenes, where the peak positions of C–X are determined to be: F (287.5 eV) > Cl (286.3 eV) > Br (286.0 eV) > I (285.8 eV) [5,22].

The question arises if the ring position of the substituent X in the halogenated benzoic acids will influence the peak position in the NEXAFS. Therefore, the spectra of 2-halogen substituted benzoic acids (X = F, Cl, Br and I) and 3-iodobenzoic acid are recorded (not shown). The peak positions are summarized in Table 2. No significant influence of the ring position on the C 1s-NEXAFS peak positions is detected.

The qualitative spectral trends for these compounds are in agreement with previous NEXAFS 'functional group fingerprinting' interpretations. The analysis of NEXAFS spectra in terms of 'building blocks' requires that the spectra of the sub-units are not significantly perturbed by the specific electronic environment. This is the case for the C–X peak positions in the halogenated benzoic acids, where the halogen substituents can be regarded as simple electron withdrawing point charges.

3.2. NEXAFS spectra and STXM images of Me^{n+}–PAA complexes

The C 1s-NEXAFS spectra of Na(I)-, Tb(III)-, Zr(IV)- and U(VI)–PAA are displayed in Fig. 3. The discrete part of the C 1s-NEXAFS of Na(I)–PAA is dominated by the prominent C 1s (COOH) → $\pi^*_{C=O}$ transition at ∼288.4 eV (carboxylic peak *C*, Fig. 3). All Me^{n+}–PAA samples exhibit a strong decrease in the C 1s (COOH) → $\pi^*_{C=O}$ tran-

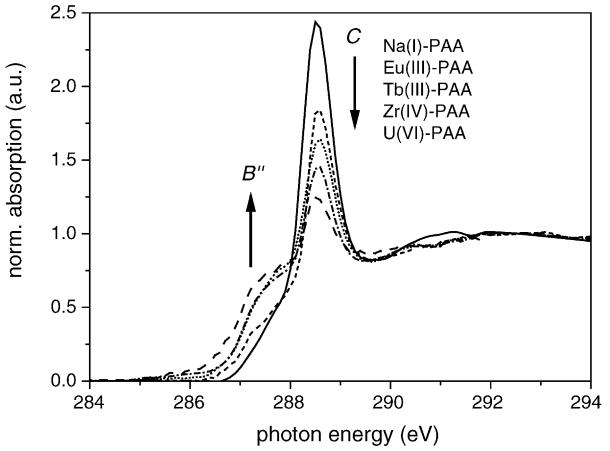

Fig. 3. Normalized C 1s-NEXAFS spectra of Na(I)-, Eu(III)-, Tb(III)-, Zr(IV)- and U(VI)–PAA (peaks *C′* decrease and *B′′* increase within this order; see text).

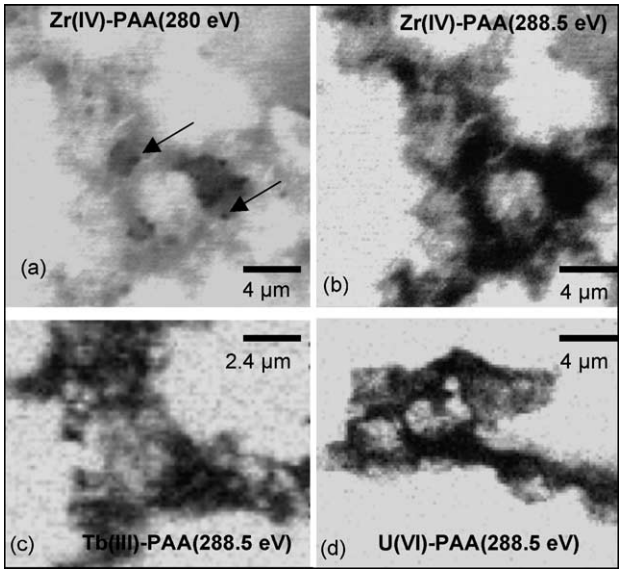

Fig. 4. STXM images of: (a) Zr(IV)–PAA at 280 eV, (b) 288.5 eV, (c) Tb(III)–PAA and (d) U(VI)–PAA both at 288.5 eV (see text).

sition intensity compared to that of Na(I)–PAA (Fig. 3, peak positions are listed in Table 3). At the same time, a broad absorption feature above 286.5 eV appears adjacent to the carboxyl resonance (*B′′* in Fig. 3). The decrease of the C 1s (COOH) → $\pi^*_{C=O}$ peak intensity of Me^{n+}–PAA complexes (compared to that of Na(I)–PAA) is in the order Eu(III) < Tb(III) < Zr(IV) < U(VI). The corresponding intensity increase of feature *B′′* is in the reverse order.

For a number of polymer samples, radiation damage during image acquisition is reported to cause distinct changes in the C 1s-NEXAFS as a result of the decomposition of the polymer [23]. Because no loss in optical density is observed for the 'coarse' low resolution NEXAFS spectra recorded before and after each high resolution spectrum for all Me^{n+}–PAA samples (see Section 2), we exclude radiation damage to cause the spectral changes observed in the PAA/Me^{n+}–PAA system. This is in agreement with our previous results [9].

The decrease in C 1s (COOH) → $\pi^*_{C=O}$ transition intensity and the feature appearing near 287.5 eV are a direct result of metal cation complexation. That a systematic trend in the intensity of these features with metal cation oxidation state is observed supports this conclusion. The intensity changes induced by the different Me^{n+} are likely to be effected by the complex structure and the character of Me^{n+}–PAA chemical bonds, which determine the complex formation constant. The complex formation constant for U(VI)–PAA is reported to be orders of magnitude higher than for Eu(III)–PAA [24,25].

The STXM images of the Me^{n+}–PAA aggregates (Fig. 4) exhibit a fractal morphology similar to that reported for Eu(III)–PAA [9]. In Fig. 4a and b, STXM images of Zr(IV)–PAA taken at 280 eV (pre-edge range) and 288.5 eV (carboxyl band) are compared. The pre-edge energy image (Fig. 4a) shows a large aggregate with embedded spots of particularly dense material (marked by arrows). These spots are not observed for the other Me^{n+}–PAA aggregates and are probably not due to carbonaceous material. They are likely particulate Zr(IV) oxo/hydroxide species forming from hydrolyzed Zr^{4+} under the pH and concentration applied in this experiment. The signature of the NEXAFS spectra

Table 3
Peak assignments and energy positions (in eV) for C 1s → π^* transitions of the Me^{n+}–PAA and Me^{n+}–HA complexes

Peak assignment (energy ranges in Figs. 3 and 5)	C=C (*A*)	C–OH (*B′*)	Complexation[a] (*B′′*)	C=O (*C*)
Na(I)–PAA	–	–	–	288.5
Eu(III)–PAA	–	–	~287.5	288.5
Tb(III)–PAA	–	–	~287.5	288.5
U(VI)–PAA	–	–	~287.5	288.5
Zr(IV)–PAA	–	–	~287.5	288.5
Eu(III)–HA (light zones)[b]	284.9	286.5		288.4
Eu(III)–HA (dark zones)[b]	284.9	286.5	287.4	288.4
U(VI)–HA (signature I)	285.0	286.6	–	288.5
U(VI)–HA (signature II)	285.0	286.6	287.4	288.5
Th(IV)–HA	285.0	286.7	287.8	288.5

[a] This peak is probably affected by metal ion complexation.
[b] From Ref. [9].

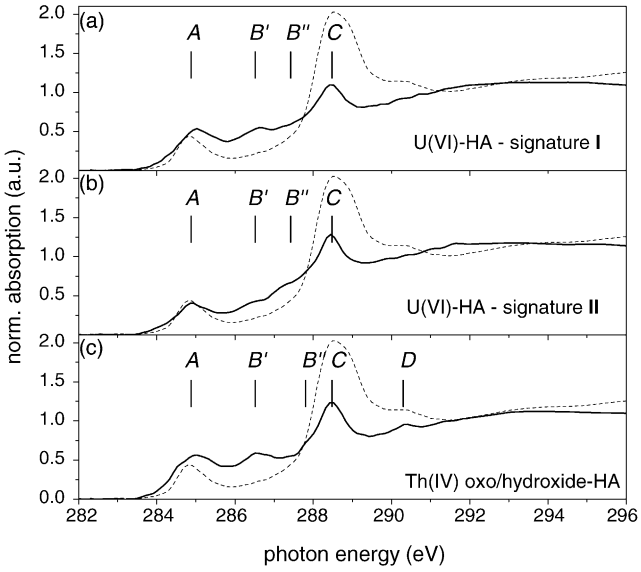

Fig. 5. Normalized C 1s-NEXAFS spectra of: (a) U(VI)–HA extracted from aggregate in Fig. 6b, (b) from aggregate in Fig. 6c, and (c) from HA coated Th(IV) oxo/hydroxide depicted in Fig. 6d. The spectrum of HA before metal loading (dashed line) is plotted for comparison (data taken from Ref. [9]).

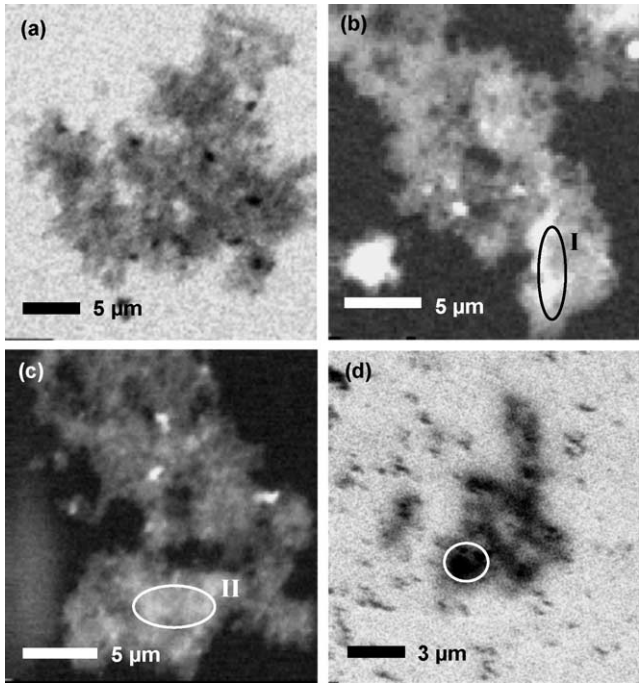

Fig. 6. (a) STXM image of U(VI)-HA at 288.5 eV, (b and c) STXM ratio images of U(VI)-HA aggregates in the spectral region of the carboxyl resonance ($-\log[I(\Delta E)/I(\Delta E_0)]$, ΔE_0 = 280–283 eV, ΔE = 287.8–289.2 eV) and (d) STXM image of HA coated Th(IV) oxo/hydroxide at 288.5 eV; C 1s-NEXAFS signatures depicted in Fig. 5 are extracted from encircled areas.

extracted from dry Na(I)–PAA and the hydrated Me^{n+}–PAA aggregates is nearly independent of the location within the specimen, which points to the chemical homogeneity of these materials.

3.3. NEXAFS spectra and STXM images of U(VI)–HA and HA coated Th(IV) oxo/hydroxide

The normalized C 1s-NEXAFS spectra of HA reacted with U(VI) and Th(IV) oxo/hydroxide are depicted in Fig. 5. Peak positions are listed in Table 3. The spectrum of HA before metal loading is plotted for comparison (dashed line in Fig. 5). The corresponding morphologies of the aggregates forming upon HA–metal interaction are compared in Fig. 6. Fig. 6a shows the overall morphology of U(VI)–HA aggregates to be very similar to those previously reported for Eu(III)–HA [8]. Patches with higher optical density are embedded in a less optical dense matrix of carbonaceous material. The spatial distribution of carboxyl functional groups in the U(VI)–HA aggregate is better visualized by calculating ratio images (Fig. 6b and c). The characteristic white spots represent dense HA material of high carboxylic functionality. Similar to Eu(III)–HA [8,9], at least two different spectral signatures characterize the C 1s-NEXAFS of U(VI)–HA: signature I (Fig. 5a), exhibiting a strong phenolic resonance (position B') and signature II (Fig. 5b), showing shoulders B' and B''. The peak position B' (286.6 eV) coincides with the phenolic C 1s (C–OH) → $\pi^*_{C=C}$ transition obtained for hydroxybenzoic acid (Fig. 1). In analogy to the feature near 287.5 eV appearing in Me^{n+}–PAA NEXAFS, we attribute feature B'' to transitions following Me^{n+} complexation. Signature II is similar to the NEXAFS extracted from the embedded patches of more dense, strongly absorbing material in Eu(III)–HA. The striking similarity of the U(VI)–HA NEXAFS signatures compared to those reported in Ref. [9]—including the drastic decrease of the carboxyl resonance—point to a similar complexation mechanism, involving the same functional groups for U(VI) as for Eu(III)–HA.

The NEXAFS of HA reacted with Th(IV) oxo/hydroxide present at pH 5.3 (Figs. 5c and 6d) exhibits strong similarities to the NEXAFS previously recorded for HA co-precipitated with Eu(III) oxo/hydroxide particles [26]. The faint structures observed to surround the hetero-aggregate in Fig. 6d are at the STXM resolution limit of around 100 nm. Only a single signature, irrespective of location and material density within the hetero-aggregates, is observed. Similar to HA coated Eu(III) oxo/hydroxide, the additional weak resonance at 290.4 eV in this spectrum (position *D* in Fig. 5c) indicates the presence of carbonate in the oxo/hydroxide particles [26,27]. The B'' position (287.8 eV) for Th(IV) oxo/hydroxide reacted with HA seems to be significantly higher than for U(VI)–HA (287.4 eV). We can only speculate whether this is due to the specific interaction with the Th(IV) oxo/hydroxide species.

4. Conclusions

The present results indicate a distinct metal ion complexation effect visible in the C 1s-NEXAFS of different

Me^{n+}–PAA complexes. The simultaneous decrease of the carboxylic peak intensity and appearence of a new transition at the low energy side of the carboxylic peak arise as a result of metal ion complexation. The extent ot the spectral changes varies with the metal cation. The two observations that: (i) the trivalent cations Eu(III) and Tb(III) exhibit different spectra and (ii) U(VI) (present as the dioxo cation $(UO_2)^{2+}$) induces the strongest spectral changes indicate that a simple electrostatic model (reflecting different oxidation states) is not sufficient to explain the spectral trends. Further investigations by NEXAFS spectroscopy and other appropriate methods are required to gain additional information on the Me^{n+}–PAA structures.

The goal of this study is the transfer of NEXAFS results for model substances to HA systems. We find that the transitions *A* and *B*′ (Fig. 5) can be used as a measure of the amount of aromatic and associated electron withdrawing chemical functional groups. Peak positions and shapes can be assigned in accordance with the model compounds. The position of peak *B*′ correlates with the overall electronegativity of the aromatic substituent in substituted benzoic acids. We expect the oscillator strength of these transitions to vary due to heterogeneous distribution of structural sub-units in HA aggregates. As far as we may judge based on our investigations up to now, these transitions are not affected by metal complex formation. In contrast, from results of the Me^{n+}–PAA reference systems, we conclude the peaks *B*′′ and *C* (Fig. 5) to be sensitive to the extent and/or type of metal ion complexation by carboxyl functional groups. For a quantitative interpretation of these transitions, especially for unknown samples, varying oscillator strength for different metal ions must be considered.

To corroborate our interpretation of the C 1s-NEXAFS of HA metal cation complexation, quantum-chemical calculations are envisaged. The potential of STXM/NEXAFS investigations, capable of probing the chemical state of hydrated natural organic matter in volumes of only a few femtoliters, combined with quantum-chemical modeling should aid in our understanding and, hence, ability at predicting the complexation behavior of HA for metal cations under a variety of conditions.

Acknowledgements

We are grateful for beam-time allotment by BNL/NSLS. All data was taken using the X-1A STXM developed by the group of Janos Kirz and Chris Jacobsen at SUNY Stony Brook, with support from the Office of Biological and Environmental Research, U.S. DoE under contract DE-FG02-89ER60858, and the NSF under Grant DBI-9605045. Thanks to Dr. Ch. Marquardt for reading the manuscript. Special thanks to Sue Wirick for technical assistance with the STXM measurements.

References

[1] M.H.B. Hayes, in: P. Mac Carthy, R.L. Malcolm, R.S. Swift (Eds.), Humic Substances, vol. II, John Wiley, New York, 1989.
[2] J.I. Kim, MRS Bull. 19 (12) (1994) 47.
[3] V. Neck, R. Müller, M. Bouby, M. Altmaier, J. Rothe, M.A. Denecke, J.I. Kim, Radiochim. Acta 90 (2002) 485.
[4] A. Möri, W.R. Alexander, H. Geckeis, W. Hauser, T. Schäfer, J. Eikenberg, T. Fierz, C. Degueldre, T. Missana, Colloids Surf. A 217 (1–3) (2003) 33.
[5] S.C.B. Myneni, Rev. Mineral. Geochem. 49 (2002) 485.
[6] J. Thieme, C. Schmidt, G. Abbt-Braun, C. Specht, F.H. Frimmel, in: F.H. Frimmel, G. Abbt-Braun (Eds.), Refractory Organic Substances in the Environment, Wiley, New York, 2000.
[7] A.C. Scheinost, R. Kretzschmar, I. Christl, C. Jacobsen, Spec. Publ. R. Soc. Chem. 273 (2002) 39.
[8] M. Plaschke, J. Rothe, T. Schäfer, M.A. Denecke, K. Dardenne, S. Pompe, K.-H. Heise, Colloids Surf. A 197 (2002) 245.
[9] M. Plaschke, J. Rothe, M.A. Denecke, T. Fanghänel, J. Electron Spectrosc. Relat. Phenom. 135 (2004) 53.
[10] M.A. Denecke, D. Bublitz, J.I. Kim, H. Moll, I.J. Farkes, Synchrotron Radiat. 6 (1999) 394.
[11] M.A. Denecke, T. Reich, S. Pompe, M. Bubner, K.-H. Heise, H. Nitsche, P.G. Allen, J.J. Bucher, N.M. Edelstein, D.K. Shuh, K.R. Czerwinski, Radiochim. Acta 82 (1998) 103.
[12] J.I. Kim, G. Buckau, G.H. Li, H. Duschner, N. Psarros, Fresenius J. Anal. Chem. 338 (1990) 245.
[13] U. Neuhäusler, S. Abend, C. Jacobsen, G. Lagaly, Colloid Polym. Sci. 277 (1999) 719.
[14] C. Jacobsen, S. Williams, E. Anderson, M.T. Browne, C.J. Buckley, D. Kern, J. Kirz, M. Rivers, X. Zhang, Opt. Commun. 86 (1991) 351.
[15] S. Spector, C. Jacobsen, D. Tennant, in: J. Thieme, G. Schmahl, E. Umbach, D. Rudolph (Eds.), X-ray Microscopy and Spectromicroscopy, Springer, Berlin, Heidelberg, 1998.
[16] C. Jacobsen, G. Flynn, S. Wirick, C. Zimba, J. Microsc. 197 (2) (2000) 173.
[17] L.G. Parratt, C.F. Hempstead, E.L. Jossem, Phys. Rev. 105 (4) (1957) 1228.
[18] B.K. Agarwal, X-Ray Spectroscopy, Springer Series in Optical Sciences, vol. 15, Springer, Berlin, Heidelberg, 1991.
[19] A.P. Hitchcock, D.C.J. Mancini, Electron. Spectrosc. 67 (1994) 1.
[20] Periodensystem der Elemente, VCH Verlagsgesellschaft, Weinheim, Germany.
[21] http://www.knowitall.com/handbook/cnmr/carboxylic_acids/aromatic/aromatic.htm.
[22] A. Benitez, J.H. Moore, J.A. Tossel, J. Chem. Phys. 88 (11) (1988) 6691.
[23] T. Coffey, S.G. Urquhart, H. Ade, J. Electron Spectrosc. Relat. Phenom. 122 (2002) 65.
[24] T. Kukota, O. Tochiyama, K. Tanaka, Y. Niibori, Radiochim. Acta 90 (2002) 569.
[25] D. Leroy, L. Martinot, C. Jérôme, R. Jérôme, Polymer 42 (2001) 4589.
[26] J. Rothe, M. Plaschke, M.A. Denecke, Radiochim. Acta 92 (2004) 711.
[27] J. Stöhr, NEXAFS Spectroscopy, Springer-Verlag, Berlin, Heidelberg, 1992.